aerospace

MDPI

Article

Parametric Study of Guidance of a 160-mm Projectile Steered with Lateral Thrusters

Robert Głębocki † and **Mariusz Jacewicz** *,†

Faculty of Power and Aeronautical Engineering, Warsaw University of Technology, 00-665 Warsaw, Poland; rglebocki@meil.pw.edu.pl
* Correspondence: mjacewicz@meil.pw.edu.pl
† These authors contributed equally to this work.

Received: 11 April 2020; Accepted: 19 May 2020; Published: 21 May 2020

Abstract: The development of projectile guidance requires consideration of a large number of possible flight scenarios with various system parameters. In this paper, the Monte-Carlo parametric study for a 160 mm artillery rocket equipped with a set of 34 small, solid propellant lateral thrusters located before the center of mass was evaluated to reduce projectile dispersion and collateral damage. The novelty of this paper lies in the functionality of modifying the shape of the trajectory in the terminal phase using lateral thrusters only. A six degree of freedom mathematical model implemented in MATLAB/Simulink was used to investigate the influence of numerous parameters on the resulting accuracy at several launch elevation angles. Augmented impact point prediction guidance was applied in the descending portion of the flight trajectory to achieve the trajectory shaping functionality. The optimum combination of thruster magnitude and algorithm parameters was obtained. The real data from the LN200 inertial measurement unit were used to investigate the influence of noise on the resulting accuracy. It was shown that with the proposed guidance method, the dispersion could be reduced by more than 250 times and the projectile impact angle might be increased when compared to an unguided projectile.

Keywords: Monte-Carlo; lateral thruster; rocket artillery; dispersion; control authority

---

1. Introduction

The Monte-Carlo methodology is currently extensively used for the model-based design of projectiles [1]. This approach allows researchers to investigate the influence of various parameters of the projectile configuration on the resulting performance. The main drawback of this method is that it is computationally very expensive. Therefore, full analysis for various parameters combinations is difficult to execute on a typical desktop computer, especially using a single core only. One of the most important issues in conducting such a numerical experiment is to achieve a low-cost solution to improve the speed of calculations. The main requirement for this kind of methodology is to realize a large number (order of thousands) of simulation samples in the shortest possible time.

In missile technology, there are various fields of applications of this method. Al-Garni et al. [2] presented aerodynamic shape optimization of the supersonic missile. Mihailescu et al. [3] evaluated dispersion analysis for a fire extinguishing rocket for various launch angles. The Graphic Processing Unit (GPU) was successfully adopted by Ilg et al. [4–6] for the investigation of projectile dispersion. Parametric analysis for lateral motor controlled artillery projectile was described by Pavković et al. [7–9]. A similar Monte-Carlo parametric study for mortar round with a pulse jet control mechanism was presented by Pavić et al. [10].

To assess the guidance, navigation and control (GN&C) performance, a detailed analysis should be made at the early design phase. In this way, the cost of system development might be significantly reduced.

There exist various disturbances which might affect the motion of the projectile, for example: main motor thrust misalignment, fin cant angle, launch tube vibrations, aiming errors, mass deviations from its nominal values and wind shear. Unguided rocket artillery has strong firepower but is characterized by significant dispersion [11], so it is usually used as an area weapon. To reduce the dispersion and the resulting collateral damage, various kinds of actuator have been proposed so far: movable fins [12–14], roll decoupled canards [15,16], lateral thrusters [7,9,17–19] translating internal mass [20] and drag brakes [21]. In this study, lateral thrusters were considered because this kind of actuator offers some significant advantages, such as fast response, low mass, small size and simple structure. The lack of movable parts improves actuator reliability and reduces the cost of manufacturing when compared to aerodynamic surfaces moved by electromechanical drives. With the side thrusters, both cross-range and range course corrections might be realized. Due to these reasons, the thrusters are an effective solution for projectiles where there is no need for steering during the whole flight. For instance, the AccuLAR [22] projectile uses arrays of solid propellant lateral thrusters as the only actuator to steer the rocket precisely to the target. Increasingly, the projectiles equipped with aerodynamics canards have lateral thrusters that could be used in the initial phase of flight to reduce the dispersion, such as the Ukrainian Wilcha projectile [23].

On the other hand, a limited and small number of thrusters results in low projectile maneuvering capability, which makes projectile control a challenging task. The control authority when comparing with other conventional systems is relatively low. The achievable lateral and longitudinal deflection of the impact point is typically in the order of several hundred meters [24,25]. Drescher et al. [11] reported that for a projectile steered by 32 thrusters, the 380 m lateral correction at a range of 20 km is possible. Similarly, Gao et al. [24] concluded that for 122 mm projectiles with 10 thrusters, the correction in range was 410 m, and 561 m in cross-range. Corriveau et al. [25] showed that for the 105 mm artillery projectile steered by five thrusters, drift correction equal to only 247.8 m might be achieved. The footprint of projectiles that use the discontinuous actuators, such as pulse thrusters, is often significantly smaller than for munition equipped in continuously operating devices like canards [17].

Three kinds of guidance method are commonly used for low control authority projectiles [26,27]: trajectory tracking, impact point prediction and trajectory shaping. In the trajectory tracking (TT) approach, the projectile flies along the prespecified path [28,29]. Jitpraphai et al. [30] compared TT and proportional navigation. Impact point prediction (IPP) guidance is realized by evaluating the projectile's dynamics from its current state to ground impact and generating the control inputs according to the differences between the calculated and desired point of impact to reduce the miss distance [31,32]. Prediction of the future projectile state is quite a computationally expensive task [33,34]. For this reason, various impact point predictors were developed to simplify the computations [35,36]. Linear theory and modified linear theory were presented in [37,38]. Various impact predictors were compared by Fresconi et al. [39]. In trajectory shaping (TS), not only is the miss distance minimized, but also some additional quantity, e.g., the direction of the velocity vector of the projectile at impact, might be controlled [40]. Generalized vector explicit guidance (GENEX) and forward integration of terminal states (FITS) were investigated by Pamadi et al. [41]. These methods might be applicable when sufficient control authority is available, so they are intended for use with aerodynamic steering devices rather than lateral motors. The main challenge in using TS for rocket artillery equipped in pulse actuator is to overcome the munition limited maneuverability. To achieve larger correction capabilities, the number of thrusters and thrust magnitude might be increased, but this is not always possible. The number of thrusters is restricted by the size of the projectile. In turn, the increasing of thruster magnitude results in large angular oscillations [42,43]. The use of the trajectory shaping method for lateral thrusters steered projectiles is not mature and requires further investigations.

This paper introduces several novelties. The main contribution of this work is the methodology of conducting Monte-Carlo simulations intended for practical design purposes of lateral thruster steered projectiles. A large set of uncertainties was included in the analysis. To assess the minimum lateral thruster magnitude and to evaluate the effectiveness of the proposed guidance method, a parametric study of the algorithm was performed. Second, the trajectory shaping guidance intended for using lateral thrusters as actuators was successfully investigated. The presented numerical results indicate that the projectile effectiveness could be increased significantly when compared to the unguided case.

This paper is organized as follows. Section 2 presents the test platform, the developed mathematical model and the guidance algorithm. Section 3 includes the results of numerical simulations. The contribution ends with a summary of the most important conclusions.

2. Materials and Methods

2.1. The Test Platform

The existing 160 mm surface-to-surface rocket (Figure 1) was used as an example test platform for simulation purposes.

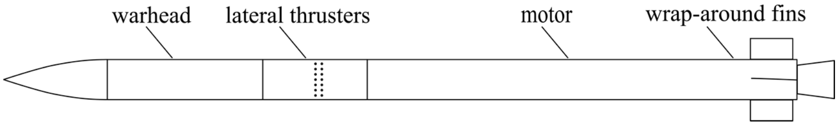

Figure 1. Configuration of the 160 mm projectile.

The basic projectile parameters were assumed according to [22]. The reverse engineering method was applied to obtain some unknown data. The rocket was assumed to be a variable mass, axisymmetric rigid body with six degrees of freedom (6DoF). The projectile length is 3.4 m, the mass before/after main motor burnout is m_0 = 110 kg/m_k = 66 kg and the projectile center of gravity location is x_{cgo} = 1.9 m/x_{cgk} = 2.2 m from the missile base. The initial moments of inertia are I_{xx0} = 0.5 kgm^2 and I_{yy0} = I_{zz0} = 64 kgm^2. Inertia parameters after main motor burnout are I_{xx0} = 0.4 kgm^2 and I_{yyk} = I_{zzk} = 38 kgm^2. The projectile is stabilized with four rectangular, wrap-around fins located at the rear part. The rocket spins around the longitudinal axis (clockwise looking from the base) due to the 0.5 fin cant angle. The main motor operation time was assumed to be 3.4 s and the total impulse 99,624 Ns. The main rocket motor thrust misalignment was included in the model. It was assumed that the projectile is equipped with a set of 34 identical solid propellant lateral thrusters spaced equally around the missile body. The nozzles of the lateral thrusters are located x_{lt} = 2.16 m from the missile base. Each of the pulse motors can generate a force perpendicular to the longitudinal axis of symmetry. The projectile maneuverability depends on the operation time of the thruster and the total impulse. The considerations presented here were limited to one, selected operation time. The thrust characteristics were assumed to be a rectangular pulse with the operation time of the thruster being 0.04 s, and amplitudes from 100 N (the total impulse of the single thruster 4 Ns) up to 2000 N (80 Ns) were considered. It was assumed that the lateral motor interference effects could be neglected. The main advantages of such a control system are the lack of movable parts, low cost and high reliability. The main difficulty in this type of actuator is that each of the thrusters could be used only once. Single channel control was considered. The roll rate of the rocket cannot be too high because in such a situation, effectiveness will be reduced. Aerodynamic characteristics were obtained with the aim of engineering level semi-empirical codes. Base drag variations due to main motor burn were included. The maximum rocket range is ≅ 40 km, so flat Earth approximation was used. Air properties were assumed according to [44].

2.2. Projectile Mathematical Model

The coordinate systems used in the simulation are presented in Figure 2.

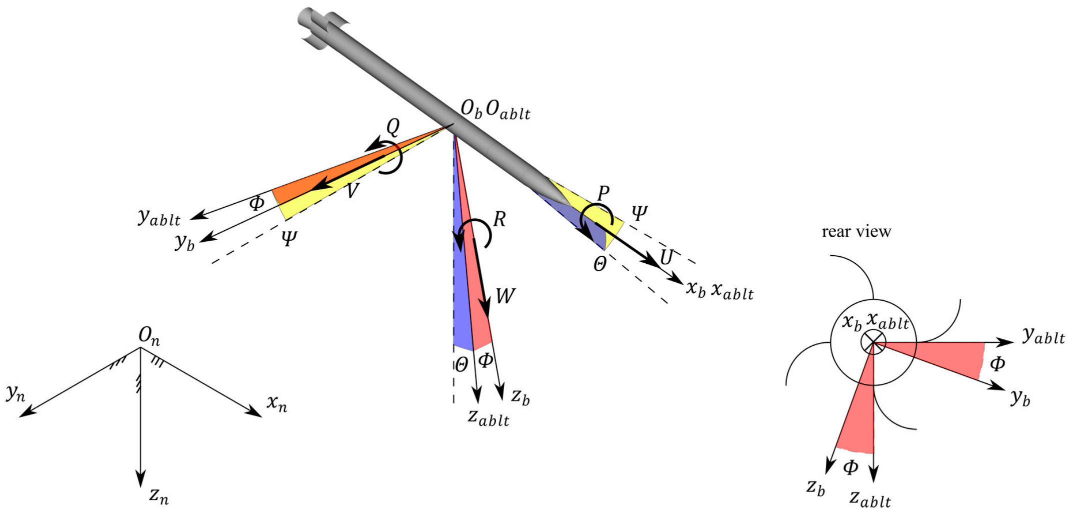

Figure 2. Coordinate systems used in the model.

The body fixed frame $O_b x_b y_b z_b$ moves forward with time while the main motor is burning the propellant. The equations of motion of the projectile are [31,45–47]:

$$\begin{bmatrix} \dot{U} \\ \dot{V} \\ \dot{W} \end{bmatrix} = \frac{1}{m}\begin{bmatrix} X_b \\ Y_b \\ Z_b \end{bmatrix} - \begin{bmatrix} 0 & -R & Q \\ R & 0 & -P \\ -Q & P & 0 \end{bmatrix}\begin{bmatrix} U \\ V \\ W \end{bmatrix} \tag{1}$$

$$\begin{bmatrix} \dot{P} \\ \dot{Q} \\ \dot{R} \end{bmatrix} = I^{-1}\begin{bmatrix} L_b \\ M_b \\ N_b \end{bmatrix} - I^{-1}\begin{bmatrix} 0 & -R & Q \\ R & 0 & -P \\ -Q & P & 0 \end{bmatrix} I \begin{bmatrix} P \\ Q \\ R \end{bmatrix} \tag{2}$$

$$\begin{bmatrix} \dot{x}_n \\ \dot{y}_n \\ \dot{z}_n \end{bmatrix} = \begin{bmatrix} \cos\Theta\cos\Psi & \sin\Phi\sin\Theta\cos\Psi - \cos\Phi\sin\Psi & \cos\Phi\sin\Theta\cos\Psi + \sin\Phi\sin\Psi \\ \cos\Theta\sin\Psi & \sin\Phi\sin\Theta\sin\Psi + \cos\Phi\cos\Psi & \cos\Phi\sin\Theta\sin\Psi - \sin\Phi\cos\Psi \\ -\sin\Theta & \sin\Phi\cos\Theta & \cos\Phi\cos\Theta \end{bmatrix}\begin{bmatrix} U \\ V \\ W \end{bmatrix} \tag{3}$$

$$\begin{bmatrix} \dot{\Phi} \\ \dot{\Theta} \\ \dot{\Psi} \end{bmatrix} = \begin{bmatrix} 1 & \sin\Phi\tan\Theta & \cos\Phi\ \tan\Theta \\ 0 & \cos\Phi & -\sin\Phi \\ 0 & \sin\Phi/\cos\Theta & \cos\Phi/\cos\Theta \end{bmatrix}\begin{bmatrix} P \\ Q \\ R \end{bmatrix} \tag{4}$$

where U, V, W are linear velocities in the body frame, P, Q, R are angular rates, x_n, y_n, z_n represent the location of the projectile center of mass and Φ, Θ, Ψ are Euler angles. m is the projectile mass and $I = \mathrm{diag}\left(I_{xx}, I_{yy}, I_{zz}\right)$ is the inertia matrix where I_{xx}, I_{yy}, I_{zz} are moments of inertia. X_b, Y_b, Z_b are forces and L_b, M_b, N_b are moments in the body fixed frame. The dot symbol above variables means a first derivative with respect to time.

The forces $F_b = \begin{bmatrix} X_b & Y_b & Z_b \end{bmatrix}^T$ acting on the projectile in the body frame were computed as [48]:

$$F_b = F_g + F_m + F_a + F_{lt} \tag{5}$$

where F_g are gravity, F_m propulsive, F_a aerodynamic and F_{lt} lateral motors generated loads. In a similar way, moments $M_b = \begin{bmatrix} L_b & M_b & N_b \end{bmatrix}^T$ with respect to the center of mass were calculated as:

$$M_b = M_g + M_m + M_a + M_{lt} \tag{6}$$

The gravity forces were calculated as follows:

$$F_g = mg \begin{bmatrix} -\sin\Theta \\ \sin\Phi\cos\Theta \\ \cos\Phi\cos\Theta \end{bmatrix} \tag{7}$$

where g is gravity acceleration. It was assumed that the origin of the body fixed frame $O_b x_b y_b z_b$ coincides with the projectile center of mass, which implies that $M_g = \begin{bmatrix} 0 & 0 & 0 \end{bmatrix}^T$.

The main motor forces were calculated as:

$$F_m = T_m(t) \begin{bmatrix} \cos\Psi_\mathrm{T}\cos\Theta_\mathrm{T} \\ \cos\Theta_\mathrm{T}\sin\Psi_\mathrm{T} \\ -\sin\Theta_\mathrm{T} \end{bmatrix} \tag{8}$$

where T_m is the main motor thrust force. The propulsive moments were obtained as:

$$M_m = \begin{bmatrix} -x_{cg}(t) \\ 0 \\ 0 \end{bmatrix} \times T_m(t) \begin{bmatrix} \cos\Psi_\mathrm{T}\cos\Theta_\mathrm{T} \\ \cos\Theta_\mathrm{T}\sin\Psi_\mathrm{T} \\ -\sin\Theta_\mathrm{T} \end{bmatrix} \tag{9}$$

Aerodynamic forces were calculated as:

$$F_a = \frac{1}{2}\rho V_0^2 S \begin{bmatrix} C_X \\ C_Y \\ C_Z \end{bmatrix} \tag{10}$$

where ρ is the air density, V_0 is the projectile velocity, S is the cross section area, and d is the projectile diameter. C_X, C_Y, C_Z are axial, side and normal force coefficients, respectively. Moments were obtained as:

$$M_a = \frac{1}{2}\rho V_0^2 S d \begin{bmatrix} C_L + C_{LP}\frac{P}{2V_0} \\ C_M + C_{MQ}\frac{Q}{2V_0} \\ C_N + C_{NR}\frac{R}{2V_0} \end{bmatrix} \tag{11}$$

where C_L, C_M,C_N are roll, pitch and yaw moments coefficients. C_{LP}, C_{MQ} and C_{NR} are roll, pitch and yaw damping coefficients.

The force generated by lateral motors was calculated as a sum of forces from individual thrusters [28]:

$$F_{lt} = \sum_{i=1}^{N} T_{sk}(t) \begin{bmatrix} 0 \\ \sin(2\pi(i-1)/N) \\ -\cos(2\pi(i-1)/N) \end{bmatrix} \tag{12}$$

where i is the number of thruster, N is the total number of thrusters and T_{sk} is the magnitude of the single thruster control force. The moments were calculated as a cross product between the distance of the center of mass and the thrusters location:

$$M_{lt} = \begin{bmatrix} x_{lt} - x_{cg} \\ 0 \\ 0 \end{bmatrix} \times \sum_{i=1}^{N} T_{sk}(t) \begin{bmatrix} 0 \\ \sin(2\pi(i-1)/N) \\ -\cos(2\pi(i-1)/N) \end{bmatrix} \tag{13}$$

Due to short operation times, the thrust magnitude was assumed to be constant.

2.3. Combined Prediction and Trajectory Shaping Guidance

The projectile is indirect fire and single channel-controlled. An impact point prediction algorithm was developed to steer the projectile to the target. In this approach, the dynamic model of the projectile is used to obtain the coordinates of the impact point and apply the required control actions (Figure 3).

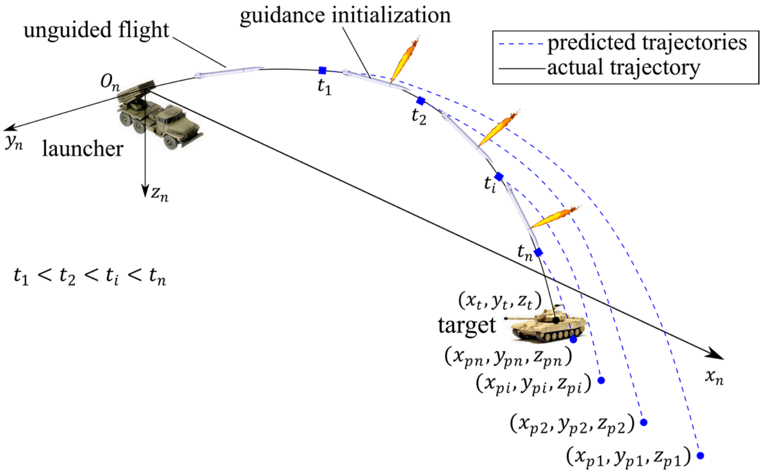

Figure 3. The concept of predictive guidance.

Zero-effort miss distance is calculated and used to achieve the target. The magnitude of the thruster force is constant for each of the motors, so the only possibility is to use pulse frequency modulation.

A set of conditions for firing the single thruster was formulated as below [8,28,49]:

- The thruster has not been consumed already
- The difference between the actual time and the last motor firing is bigger than some threshold t_{min}

$$t - t_{prev} \geq t_{min} \tag{14}$$

where t_{min} is a function of air density and was calculated as $t_{min} = \tau_{min}/\rho(h)$. It means that at low elevation angles $t_{min} \cong \tau_{min}$, but at high launch angles $t_{min} > \tau_{min}$. The projectile altitude h is estimated in real time with the onboard navigation system.
- The thruster is fired when the projectile is at a proper angular orientation (Figure 4a)

$$\left|\gamma - \Phi_i - \pi - P(\tau_{sk} + \tau_d)\right| < \varepsilon \tag{15}$$

where $0 \leq \gamma \leq 2\pi$ is the angle defining the desired flight direction, Φ_i is the angular location of the i-th thruster, P is projectile roll rate and τ_{sk} is calculated as:

$$\tau_{sk} = \frac{\int_0^{t_{lt}} T_{lt}(t)tdt}{\int_0^{t_{lt}} T_{lt}(t)dt} \tag{16}$$

where t_{lt} is operation time of the lateral rocket motor. ε is the angle threshold which defines the directional accuracy and should be as small as possible. In (15), π is subtracted from other quantities because the control force must be generated at the opposite side of the projectile fuselage than the commanded flight direction.

Next, the miss distance Δx in range and Δy in cross-range (Figure 4b) were calculated as the difference between the calculated impact point and the target coordinates [36]:

$$\Delta x = x_p - x_t \quad \Delta y = y_p - y_t \tag{17}$$

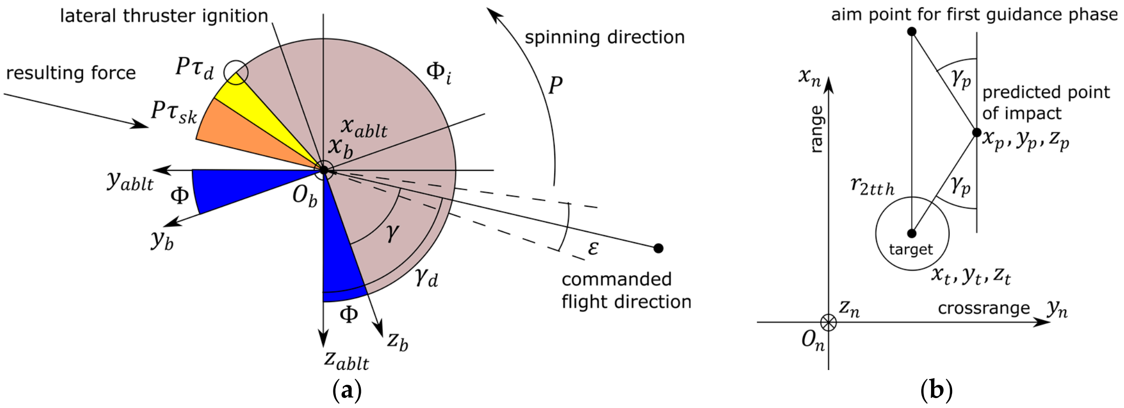

Figure 4. (**a**) Lateral thruster angular orientation; (**b**) impact point errors in the horizontal plane.

The direction of required translation γ_p in target plane is obtained from the equation:

$$\gamma_p = \mathrm{mod}(\mathrm{atan2}(\Delta y, \Delta x), 2\pi) \tag{18}$$

and modulo operation (remainder after division) is used to maintain the calculated angle in the range $0 \le \gamma_p \le 360$. The roll rate of the projectile is relatively low, so it was assumed that $\gamma_p \cong \gamma_d$. Because of the projectile spin, the commanded flight direction γ_d must be converted from non-rolling $O_{ablt}x_{ablt}y_{ablt}z_{ablt}$ to body frame $O_b x_b y_b z_b$:

$$\gamma = \mathrm{mod}(\gamma_d - \mathrm{mod}(\varPhi, 2\pi), 2\pi) \tag{19}$$

The modulo operation is used twice to provide angle values in the appropriate ranges: $0 \le \varPhi \le 360$ and $0 \le \gamma \le 360$.

- The consumption of lateral thrusters takes place only when the shell pitch angle $\varTheta$ is smaller or equal than the desired threshold $\varTheta_g$ and the flight time t is larger than t_g

$$\varTheta \le \varTheta_g \wedge t \ge t_g \tag{20}$$

Additionally, the miss distance magnitude between the target and predicted point of impact was calculated as [31]:

$$r_{2t} = \sqrt{\left(x_t - x_p\right)^2 + \left(y_t - y_p\right)^2} \tag{21}$$

- The thrusters might be fired only when $r_{2t} \ge r_{2tth}$.

r_{2tt} is the radius of the circular window centered on the target (Figure 4b). No control action is evaluated when the miss distance is smaller than the presumed value r_{2tth}. This prevents undesired consumption of thrusters early in the flight when achieving pinpoint accuracy.

Impact point prediction guidance [5developed to improve the projectile accuracy. The most accurate predictor is the 6DoF model but a highly nonlinear model is computationally expensive and requires an expensive, sophisticated onboard computer. To reduce the requirements on the hardware, simplified approaches are commonly used. The point mass model was used to calculate the missile trajectories. The equations describing the motion of the projectile in $O_n x_n y_n z_n$ are [39,50]:

$$\ddot{x}_n = -\frac{\pi \rho d^2 C_{X0} V_0}{8m}\dot{x}_n \tag{22}$$

$$\ddot{y}_n = -\frac{\pi \rho d^2 C_{X0} V_0}{8m}\dot{y}_n \tag{23}$$

$$\ddot{z}_n = -\frac{\pi \rho d^2 C_{X0} V_0}{8m} \dot{z}_n + g \tag{24}$$

where C_{X0} is the zero yaw drag coefficient, which is Mach number dependent, and V_0 is the total flight velocity. Atmosphere data according to [44] were implemented in the guidance algorithm. Equations (22)–(24) were solved using the variable step Runge–Kutta method. Measuring wind velocity is demanding, so zero wind components assumptions were introduced at the impact point prediction stage. It was assumed that the guidance starts after the trajectory vertex, because in the ascending portion of the flight, the roll rate is too high to realize the pulse corrections effectively.

One of the desired features of the munition is the capability of attack in the terminal phase from various directions. At present, military operations are often conducted in the urban environment in narrow canyons between two buildings where top attack is desired. Moreover, the warhead effectiveness depends on the angle of impact and it is much better to achieve steeper trajectory in the terminal phase of the flight. To realize this goal, the trajectory shaping capability was introduced into the algorithm. The main difficulty in achieving such a functionality lies in the fact that the lateral thrusters are used as a control mechanism and, as a result, the 160 mm test platform has very weak gliding capabilities. To overcome this difficulty, the guidance process was divided into two phases. Immediately after starting the control phase in the descending part of the trajectory, the first N_1 thrusters in the firing sequence are reserved to steer the projectile upward and extend the rocket range:

$$\text{if } n \leq N_1 \text{ then } \gamma_d = \text{mod}(\text{atan2}(\Delta y, -|\Delta x|), 2\pi) \tag{25}$$

where n is the number of already consumed thrusters. In this way, in the first phase, only lateral correction to the target is performed (Figure 4b), but the range error might be introduced intentionally. In the second phase, the projectile is steered directly to the target, so:

$$\text{if } n > N_1 \text{ then } \gamma_d = \gamma_p \tag{26}$$

The second, terminal guidance phase is initiated with some delay with respect to the end of the shaping phase, when $\Theta > \Theta_{g1}$. It was assumed that $\Theta_g \geq \Theta_{g1}$. In a special case, if $\Theta_g = \Theta_{g1}$, then the second phase starts immediately after the first. The block diagram of the guidance process is presented in Figure 5.

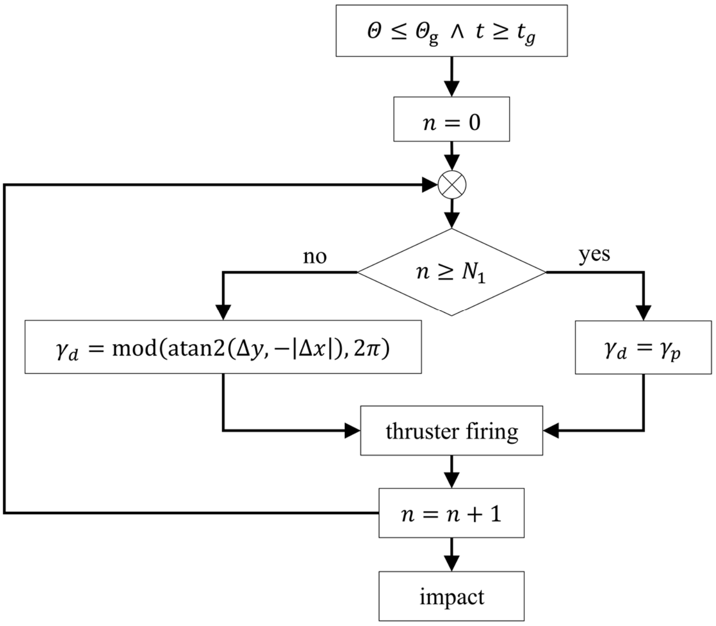

Figure 5. Guidance process with the trajectory shaping functionality.

Before the beginning of the guided flight phase, the counter is set to zero. After each side thruster fires, the counter is increased by one. The rest of the unused thrusters $N - N_1$ are spent to reduce the miss distance. The algorithm parameters and target location (obtained for example from air or satellite reconnaissance) are loaded to the projectile onboard computer memory in order to externally program equipment like the fire control unit before the launch.

2.4. Inertial Navigation System Noise

The performance of the guidance algorithm and the resulting miss distance depends on the accuracy of the navigation system. The projectile position might be obtained with INS [51]. It was assumed that the projectile is equipped with an inertial navigation system based on tactical class LN200 IMU. No additional sources of navigation information were included. The use of the onboard GPS receiver might be degraded by opponent forces by jamming. To make the simulation more realistic, the noise generated with real hardware was added in the model to the "ideal" angular rates and accelerations. Static tests (Figure 6) were performed to obtain the sensor noise.

Figure 6. LN200 inertial measurement unit during static testing.

The predicted time of projectile flight at maximum range is approximately 120 s. The registration time was 3600 s with step size of 0.005 s. In order to make the noise pseudorandom for each of the flight simulations, the 120 s window was sliding from the whole data range. The vertical accelerometer at rest measures ≅ 9.81 m/s^2 so the bias was removed for simulation purposes. The example of resulting noise is presented in Figure 7.

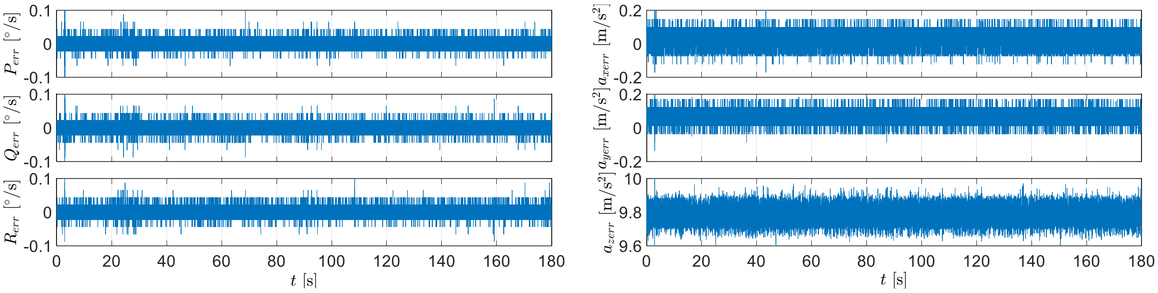

(**a**) (**b**)

Figure 7. The sensors noise obtained during static tests (**a**) gyroscopes (**b**) accelerometers.

The noise was implemented into the model using the lookup table methodology.

3. Results

The developed model was implemented in MATLAB/Simulink 2015a. The 6DoF projectile equations of motion were integrated numerically using the fixed step Runge–Kutta algorithm with a time step size of 0.0001 s.

3.1. Algorithm Test

First, two examples of the controlled flight simulation scenario are presented. The launch tube elevation angles Θ_0 in each case were set to 20° and 50°, respectively. In the second considered case, a nearly maximum projectile range is achieved. The disturbances were introduced to the nominal launch conditions (+0.1° in elevation and +0.2° in azimuth) to provoke the algorithm to take the control action. The magnitude of force generated by a single lateral thruster was assumed to be 2000 N. The minimum allowed time between two firings was set to $t_{min} = 0.5$ s and target window $r_{2tth} = 2$ m. For a nominal launch angle $\Theta_0 = 20°$, threshold pitch angles were set to $\Theta_g = 0°$ and $\Theta_{g1} = -25°$. For $\Theta_0 = 50°$, the projectile roll rate at the vertex was too high to start the guidance angle, so the parameters were set to $\Theta_g = -10°$ and $\Theta_{g1} = -50°$. The impact point prediction updating frequency was set to 10 Hz. The calculations for a single updating cycle were no longer than 130 s to prevent the guidance process from breaking. $N_1 = 10$ thrusters were used in the first guidance phase. For the preliminary tests, it was assumed that the inertial navigation system could perfectly measure or estimate the missile velocity, angular rates, position and attitude. This means, that no noise and no errors were included in the simulation. A stationary target was considered. The target is located 10 m behind the building, which constraints the angle of impact and enforces a steeper trajectory (Figure 8).

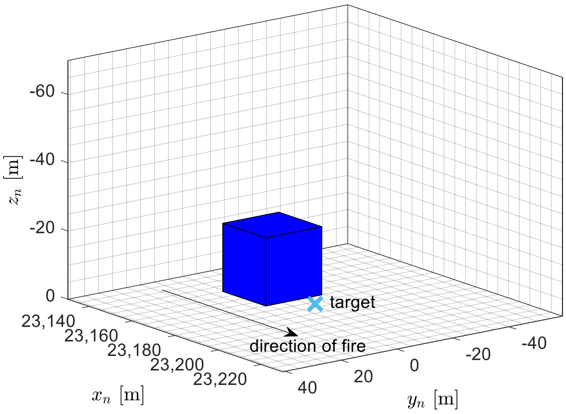

Figure 8. Simulation scenario with obstacle geometry for launch angle $\Theta_0 = 20°$.

The abovementioned scenario represents a challenging task. The inappropriate shape of the trajectory in the terminal phase might result in damaging the obstacle and cause undesired collateral damage.

The predicted trajectories for both scenarios are presented in Figure 9 (the plot was obtained by overlapping the trajectories in real time during the numerical simulation).

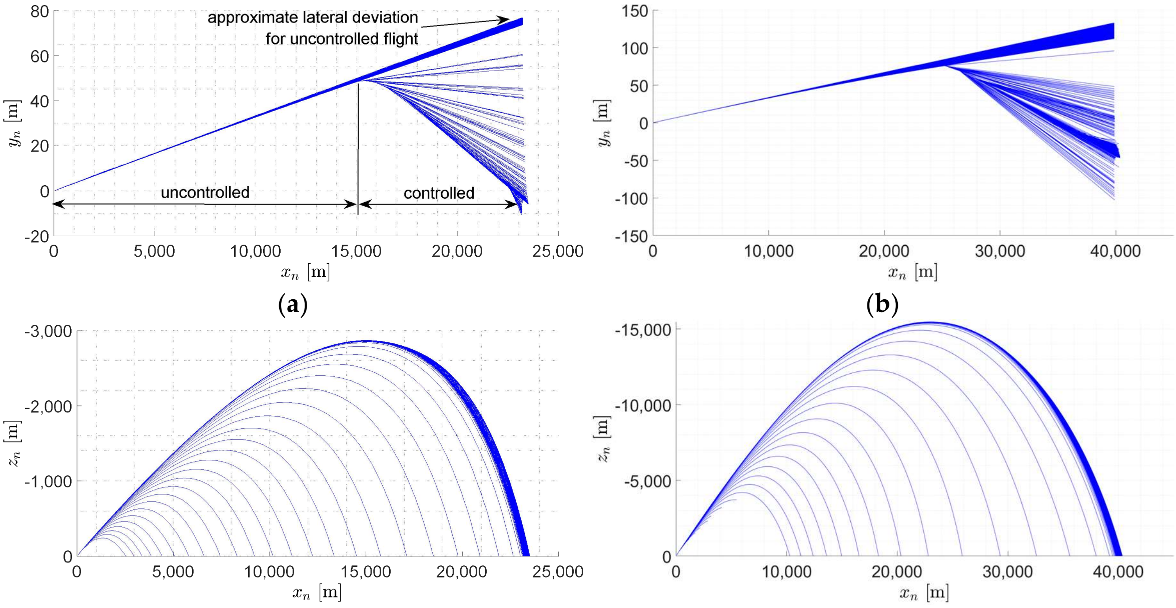

(**a**) (**b**)

(**c**) (**d**)

Figure 9. Predicted trajectories: cross-range vs. downrange for (**a**) Θ_0 = 20° (**b**) Θ_0 = 50° and altitude vs. downrange for (**c**) Θ_0 = 20° (**d**) Θ_0 = 50°.

Immediately after starting the guidance phase, the trajectories in the horizontal plane turn to the target. Additionally, from Figure 9a,b it might be seen that cross-range errors would be approximately 70 and 120 m at the end of the flight if the projectiles were uncontrolled. In the horizontal plane, a set of curves is observed because constant mass for a passive portion of the flight was implemented.

In Figure 10, the predicted impact points locations in the $O_n x_n y_n$ plane (left column) and calculated end of flight range/cross-range errors (right column) are presented.

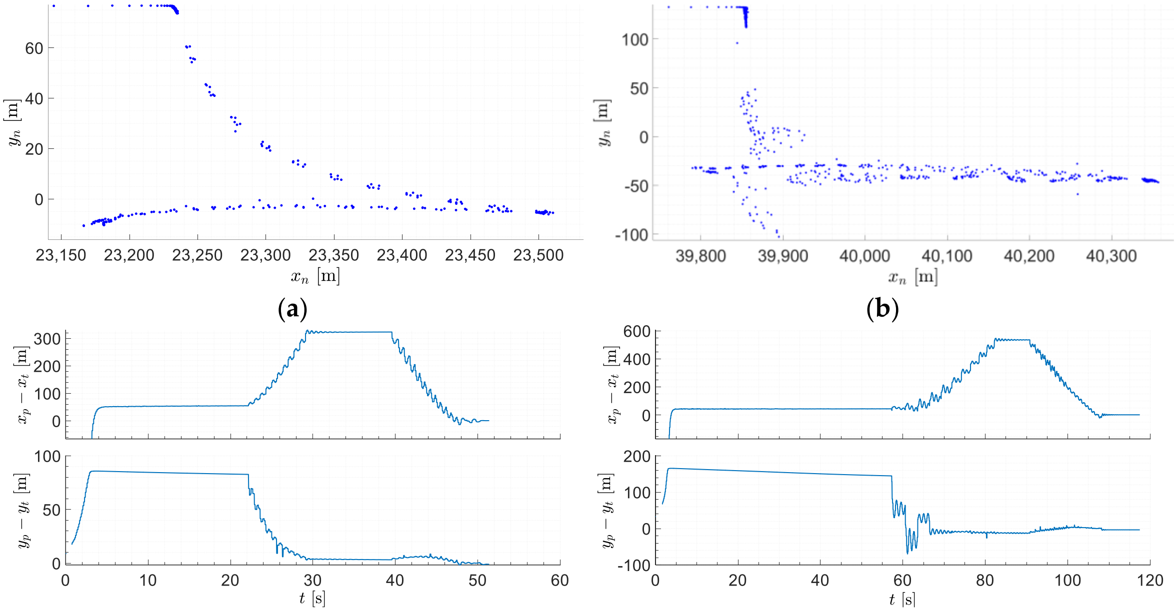

(**a**) (**b**)

(**c**) (**d**)

Figure 10. Impact point locations in the target plane (terminal phase) for (**a**) Θ_0 = 20° (**b**) Θ_0 = 50° and range/cross-range errors time history (**c**) Θ_0 = 20° (**d**) Θ_0 = 50°.

In the first guidance phase, a positive range error is introduced to make the projectile angle of the impact steepest. In the second phase, the predicted impact point locations converge rapidly to the target coordinates. The dispersion of points is the result of the numerical integration of equations of motion. The purpose is to make both errors as small as possible. Each oscillation is the result of lateral thruster firing. The range and cross-range errors are smaller than 1 m at the end of the flight.

In Figure 11, the uncontrolled and shaped trajectories are compared.

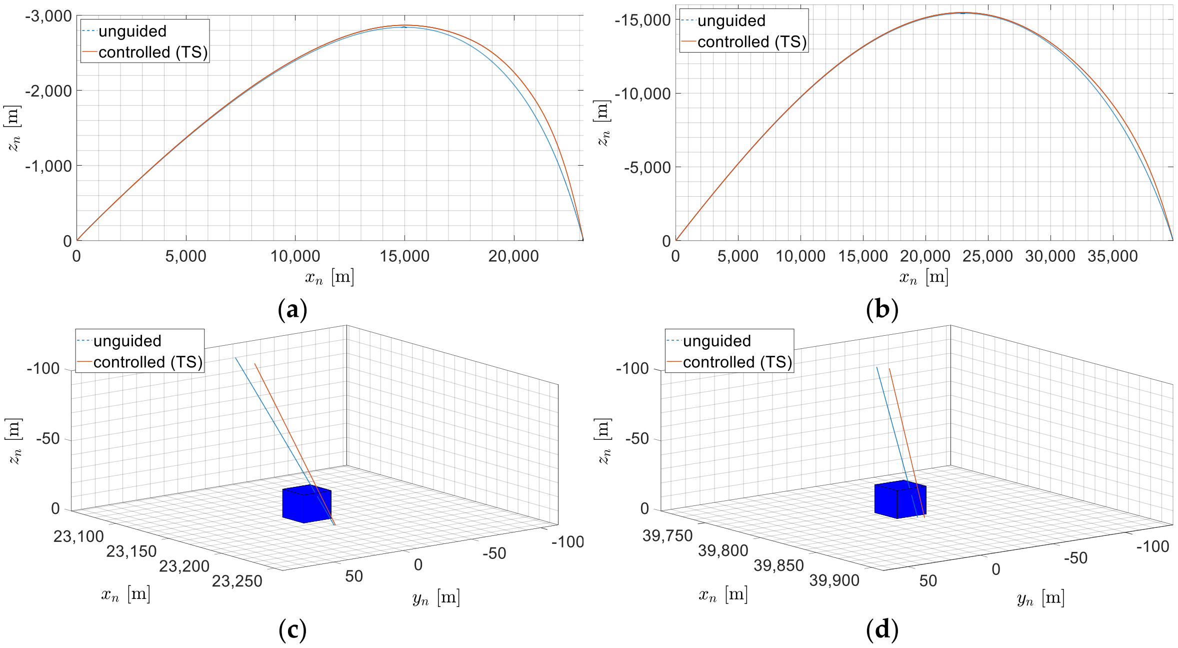

Figure 11. Trajectory shaping capabilities: altitude/cross-range vs. range (**a**) Θ_0 = 20° (**b**) Θ_0 = 50° terminal phase (**c**) Θ_0 = 20° (**d**) Θ_0 = 50°.

For launch angle 20° and uncontrolled flight, the projectile pitch angle at impact is −47.39°. As a result, the projectile falls directly into the obstacle without eliminating the target. For the controlled flight, the pitch angle was reduced to −54.03° when keeping the miss distance 1.33 m. When the projectile is launched at 50° the uncontrolled pitch angle is −69.84°, and for trajectory shaping −71.41° with a miss distance of 4.34 m. With the proposed algorithm, the target might be eliminated, preventing the obstacle from undesired damage.

In Figure 12, the total angle of attack time history is presented and the Euler angles are shown.

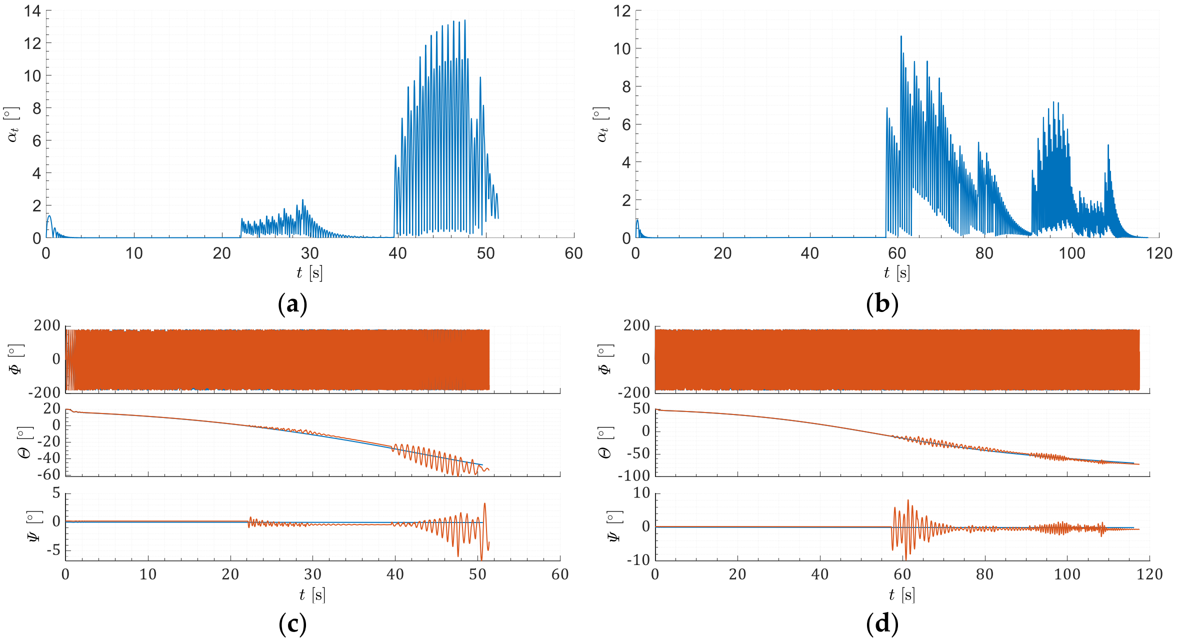

Figure 12. Total angle of attack α_t time histories (**a**) Θ_0 = 20° (**b**) Θ_0 = 50° and Euler angles vs. time (**c**) Θ_0 = 20° (**d**) Θ_0 = 50°.

The nonzero values in the initial, active phase of the flight result from the launch process. The total angle of attack increases significantly after each lateral thruster fires, but the maximum value does not exceed 13.5°, which is quite a high result for such a projectile. The control angle time history could be divided into two stages. Roll angle changes result from axial spin. Pitch and yaw angles are disturbed due to control actions.

3.2. Sensitivity Analysis

The goal of the sensitivity analysis was to investigate the influence of lateral thrust magnitude and guidance algorithm parameters on the resulting accuracy to find its most suitable combinations.

Most of the disturbances separately were modelled as a Gaussian variable. The parameters were generated using additive normal distribution. Each parameter was calculated as a sum of its nominal value and a normally distributed random variable with zero mean and some nonzero standard deviation σ. These parameters (Table 1) were assumed using the expert method and data from the literature [8,9,12,37,38].

Table 1. Parameters for the Monte-Carlo simulation.

No.	Parameter	μ	σ	Unit
1.	m_0	110	0.1	kg
2.	m_k	66	0.1	kg
3.	I_{x0}	0.5	0.03	kgm^2
4.	I_{xk}	0.4	0.03	kgm^2
5.	U_0	38	2	m/s
6.	V_0	0	1	m/s
7.	W_0	-1.7	1	m/s

Table 1. *Cont.*

No.	Parameter	μ	σ	Unit
8.	P_0	0	10	°/s
9.	Q_0	−7.5	1	°/s
10.	R_0	0	1	°/s
11.	Φ_0	0	5	°
12.	Θ_0	20/30/40/50 *	0.2	°
13.	Ψ_0	0	0.1	°
14.	Θ_T	0	0.1	°
15.	Ψ_T	0	0.1	°
16.	C_X	-	1	%
17.	C_Y, C_Z	-	0.7	%
18.	C_M, C_N	-	1	%
19.	C_{MQ}, C_{NR}	-	0.8	%
20.	T_m	-	0.5	%

* Various launch angles were considered.

The nonzero initial roll rate P_0 is realized with a rifled launch tube. The Marsenne-Twister algorithm [52] was applied to generate pseudorandom data. Circular error probable (CEP) was used to assess the accuracy of the projectile. CEP is the radius of a circle centered on the target such that 50% of the impact points lie within it [53].

The Monte-Carlo simulations were evaluated at the low-cost workstations equipped with Intel Core$^{\text{TM}}$ i7-4790 CPU @3.60 GHz with 16 GB DDR3 RAM running under Microsoft Windows 8. Using default Simulink options and a single-core CPU, one simulation of the projectile flight at the maximum range was completed in approximately 371 s, which is unacceptably long for parametric analysis. MATLAB Parallel Computing Toolbox and MATLAB Parallel Server software packages were used to speed up the calculation process. Four workstations were connected to create a small parallel server. One of the computers worked as a scheduler and three as workers. The developed computer code was optimized for speed and the simulation scenarios were evaluated parallelly using the built-in Simulink Rapid Accelerator Mode. With this option, the model execution time increased by at least several times (>10×) with respect to the Normal Mode. In this way, the available CPU cores were used more efficiently, and the total amount of time required on completing the calculation process was reduced significantly. The achieved runtime for a single simulation was approximately 21 s when the projectile was launched at the maximum range.

To obtain the minimal number of the required Monte-Carlo simulations, the following analysis was applied. At first, 3000 samples for an unguided projectile launched at $\Theta_0 = 20°$ were evaluated and the distance between the location of the mean point of impact (MPI) with respect to the target coordinates after each single simulation was calculated (Figure 13).

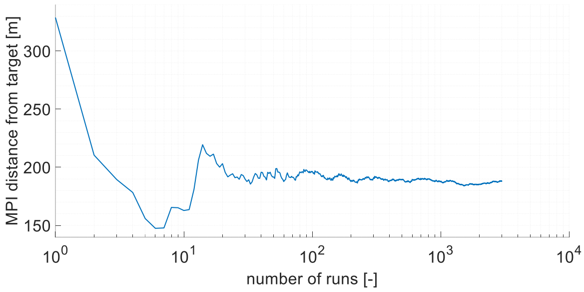

Figure 13. The mean impact point location as a function of the number of runs.

The realization of the number of simulations smaller than 100 is pointless because of the significant varying of MPI location. With more simulations, more accurate results could be obtained, but the runtime is greater. On the basis of the above results, it was decided that the number of runs cannot be smaller than 480–500. Finally, a set of 600 simulations in each considered case was evaluated.

The obtained hitting patterns for uncontrolled flight at various launch elevation angles are presented in Figure 14. It was assumed that the blast radius is 25 m and this value was marked as a green circle around the impact point. The red circle means the CEP value. The red marker in the middle of the figure is the MPI location.

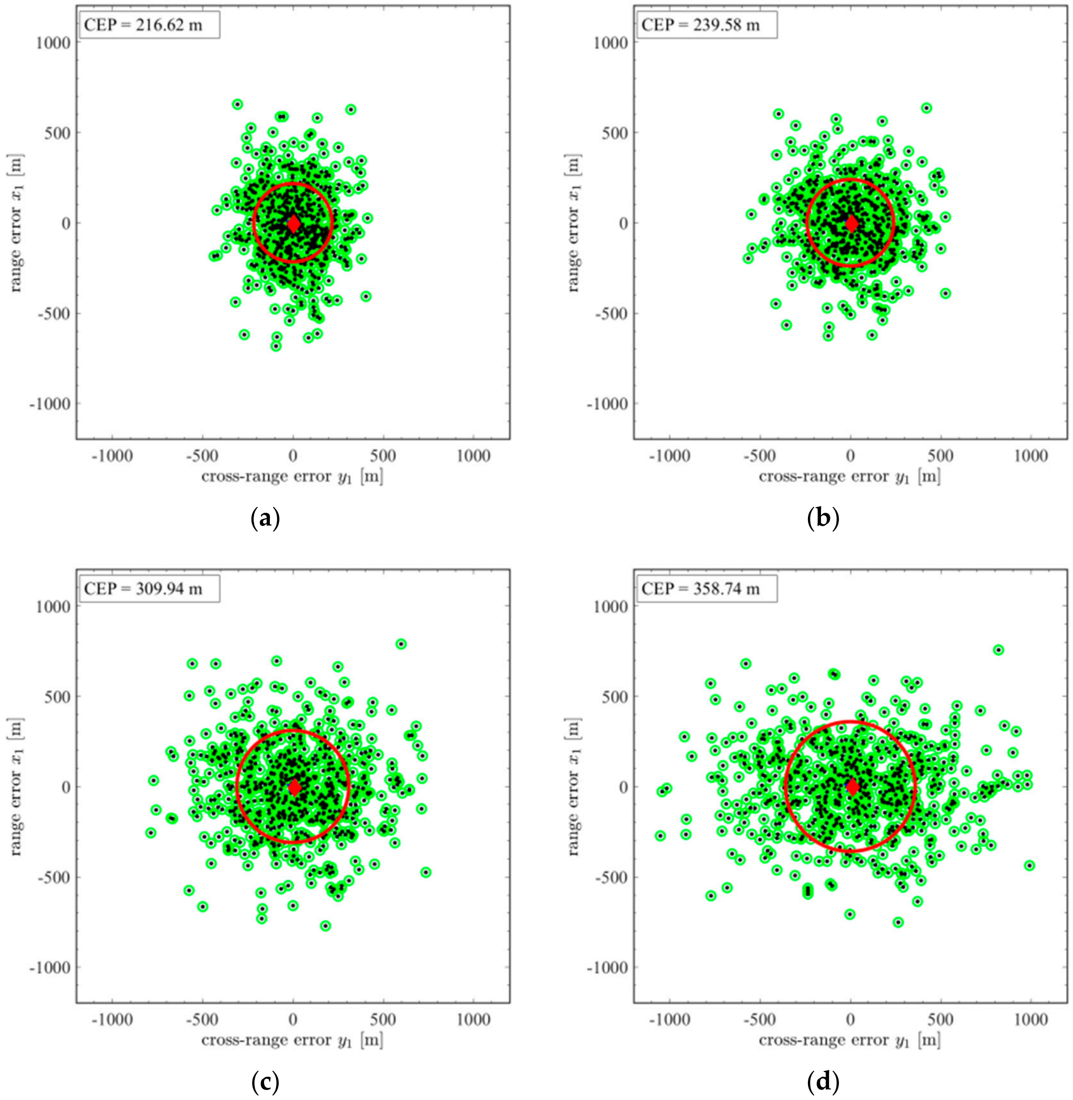

(**a**) (**b**)

(**c**) (**d**)

Figure 14. The hitting patterns for an uncontrolled projectile for various nominal launch angles (**a**) Θ_0 = 20° (**b**) Θ_0 = 30° (**c**) Θ_0 = 40° (**d**) Θ_0 = 50°.

The uncontrolled projectile has poor precision, which might result in high collateral damage. The dispersion increases with the elevation angle. At launch angle Θ_0 = 50°, lateral dispersion is higher than longitudinal. The maximum CEP is 358.74 m, achieved for the highest considered launch tube elevation Θ_0 = 50°. The obtained results indicate that with unguided munition, it is impossible to realize a precise attack.

Next, a set of open-loop controlled flight simulations was realized to obtain the projectile control authority. The thrusters were fired so as to translate the projectile in the desired radial direction maximally. The simulations were evaluated for the largest considered lateral thrust magnitude T_{sk} = 900 N and Θ_g = 0°. The thrusters were fired with t_{min} = 0.5 s. Angle γ_d was randomized from the uniform distribution with the range (0°, 360°) and fixed as constant for a single simulation. The resulting hitting patterns are presented in Figure 15.

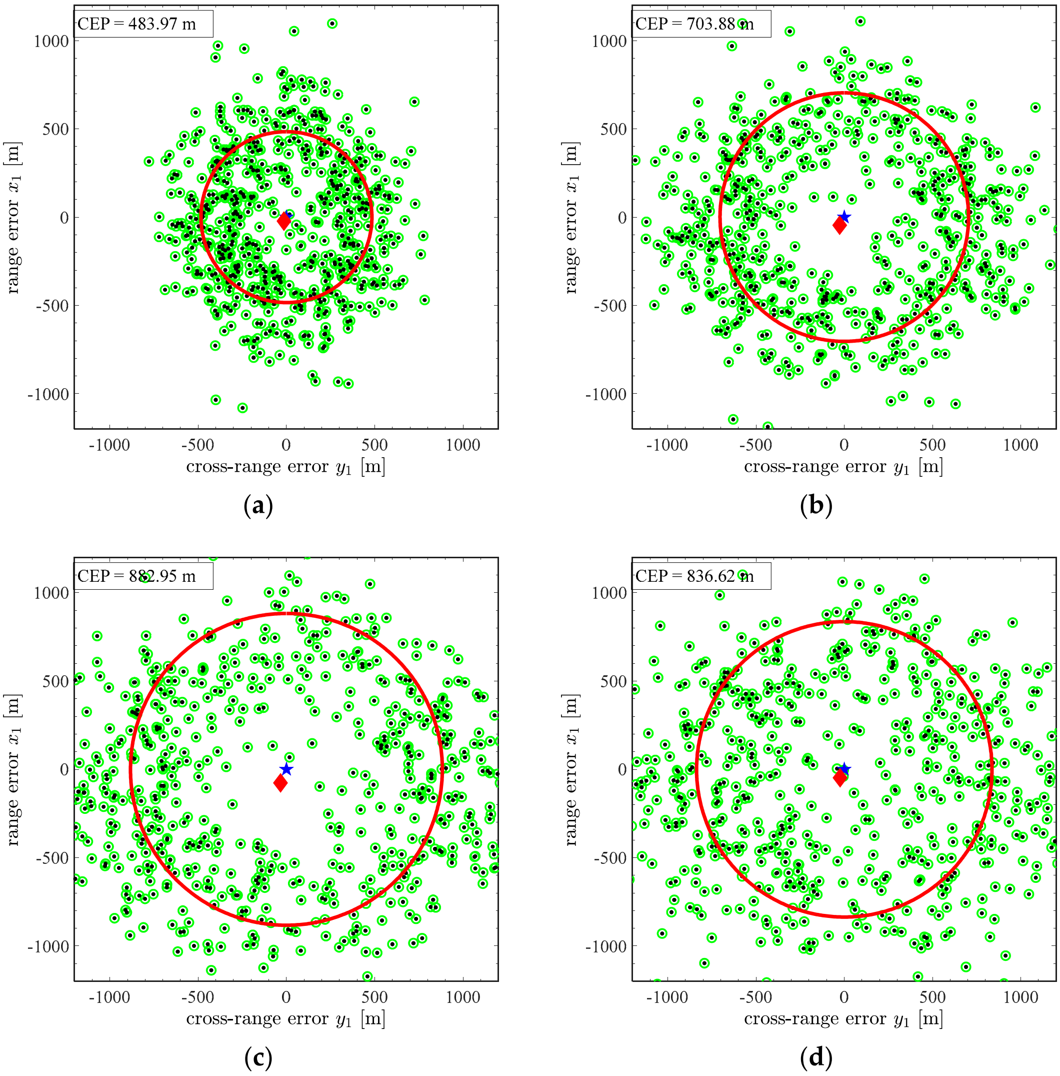

Figure 15. The projectile footprint for various nominal launch elevation angles (**a**) Θ_0 = 20° (**b**) Θ_0 = 30° (**c**) Θ_0 = 40° (**d**) Θ_0 = 50°.

The projectile is control authority limited, which is typical for this kind of guided munition. The maximum CEP is 882.95, achieved for Θ_0 = 40°. It might be expected that the largest CEP should be obtained for the maximum launch angle. The reason for these results is that the roll rate of the projectile is too high at the vertex at launch angle 50°, which degrades the correction capability.

In the next stage of the investigation, a set of closed loop simulations were performed. The trajectory shaping capability was deactivated. A single lateral thruster should be active only over a certain portion of the roll angle, for example smaller than 90°. The thruster igniter delay τ_d was assumed to be 0.002 s. The guidance algorithm parameters were fixed and set to t_g = 1 s, r_{2th} = 2 m, t_{min} = 0.5 s. Equations (22)–(24) were integrated numerically using the variable step Runge–Kutta algorithm to increase the speed of calculations. The frequency of calculations was set to 10 Hz. The influence of the lateral thruster thrust amplitude T_{sk} and threshold angle Θ_g on the resulting CEP was investigated for various launch elevation angles Θ_0. The requirements for the system were set to achieve CEP under 10 m (according to [22], as in the real system) for all considered launch angles. From the practical viewpoint, a smaller CEP is not required because the rocket warhead generates a blast which can easily eliminate the target. The calculated dispersion patterns are presented in Figures 16–19 (each axis limit is set to ±1200 m).

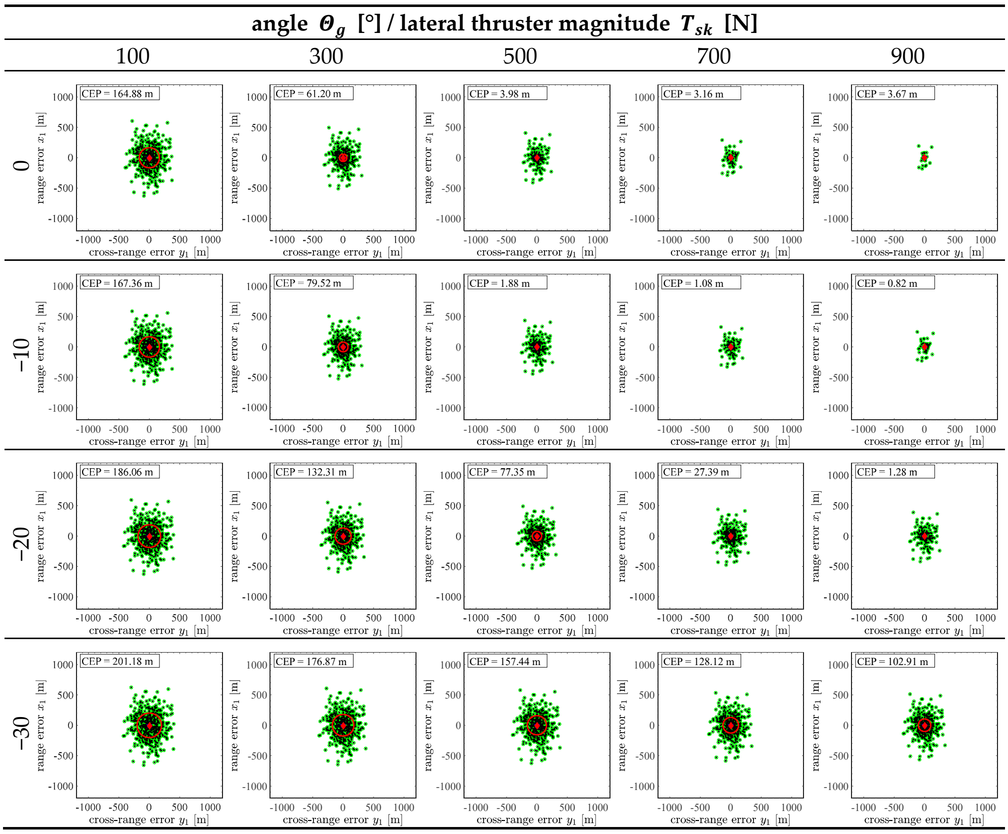

Figure 16. Dispersion patterns (nominal launch angle Θ_0 = 20°).

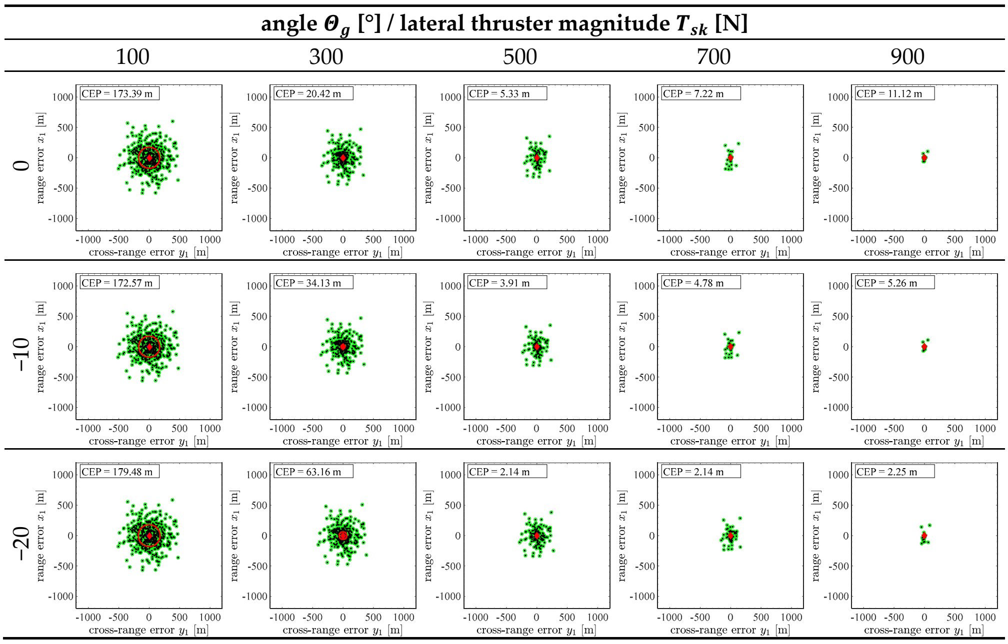

Figure 17. *Cont.*

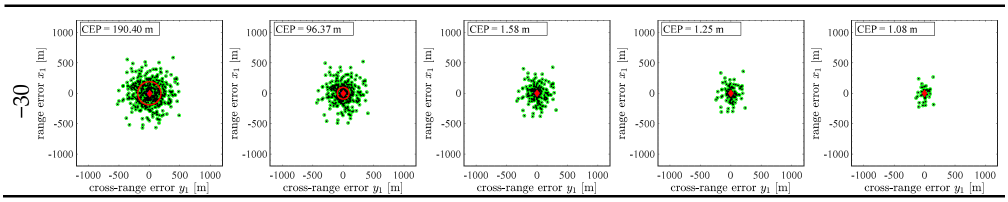

Figure 17. Dispersion patterns (nominal launch angle Θ_0 = 30°).

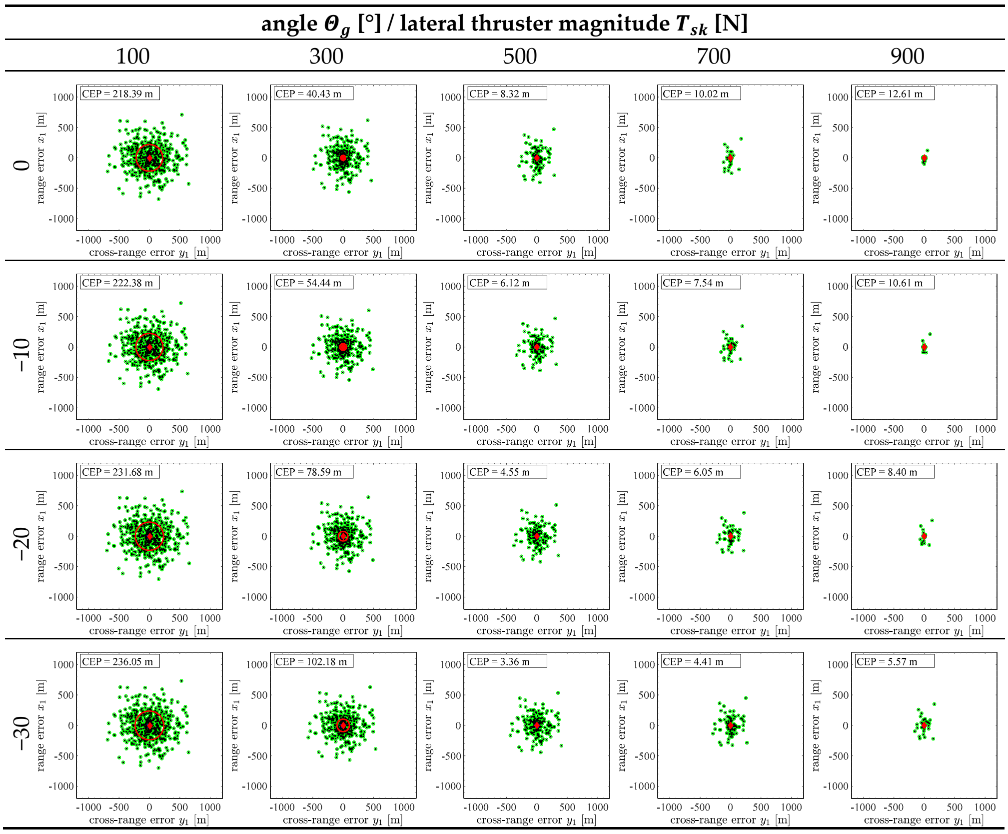

Figure 18. Dispersion patterns (nominal launch angle Θ_0 = 40°).

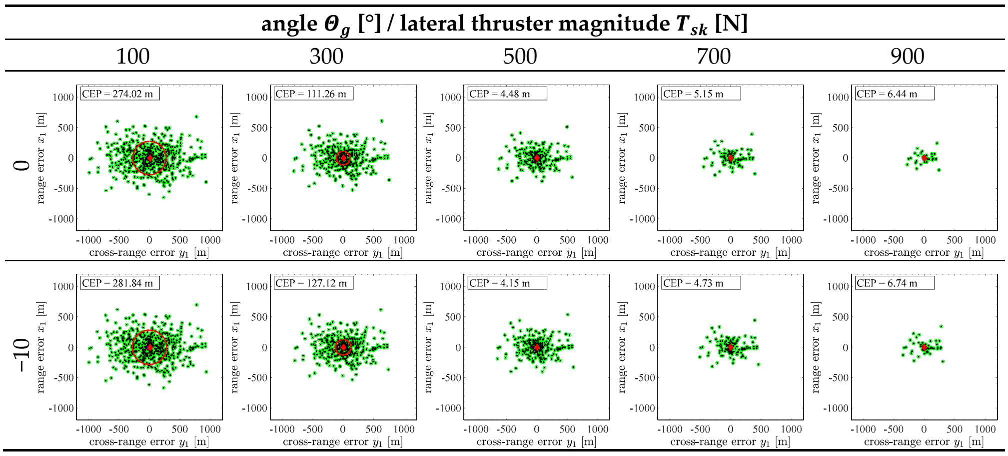

Figure 19. *Cont.*

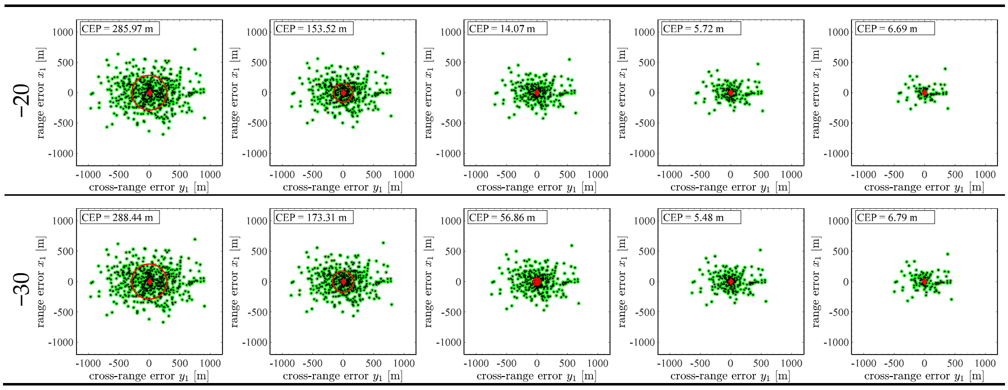

Figure 19. Dispersion patterns (nominal launch angle Θ_0 = 50°).

The obtained values of CEP are presented in Figure 20.

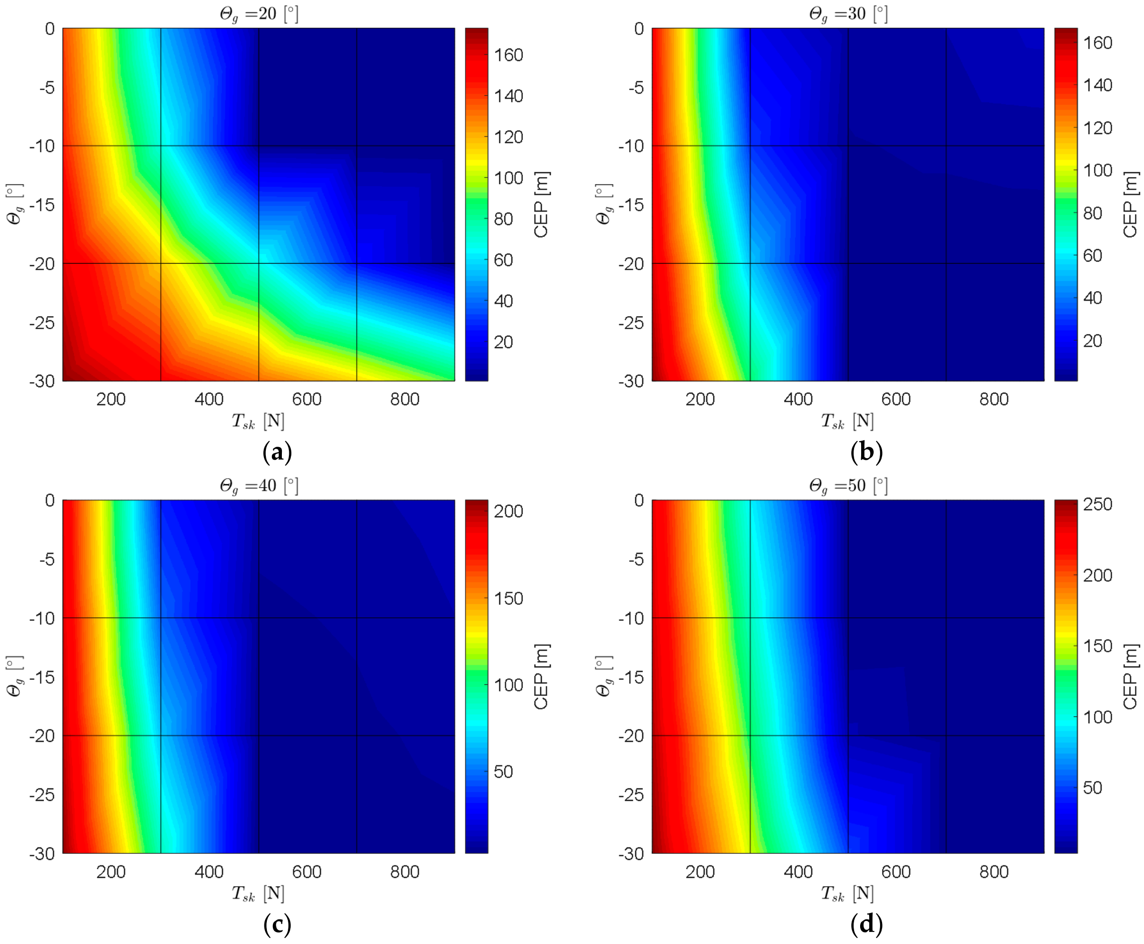

(**a**) (**b**) (**c**) (**d**)

Figure 20. Circular error probable (CEP) for various lateral pulse magnitudes T_{sk} and threshold pitch angles Θ_g as a function of the initial elevation angle (**a**) Θ_0 = 20° (**b**) Θ_0 = 30° (**c**) Θ_0 = 40° (**d**) Θ_0 = 50°.

CEP varies significantly for various combinations of T_{sk} and Θ_g. The greatest dispersion reduction is visible for changes in T_{sk} from 100 N (total impulse 4 Ns) to 300 N (12 Ns). Starting from a side force magnitude of 400 N (16 Ns), the gain from further increases is insignificant. For some combinations of system parameters, a drastic reduction in CEP is observed. The assumed earlier 10 m CEP requirement is fulfilled only for certain parameter combinations. It is impossible to achieve CEP <10 m when the thrust force is equal or smaller than 300 N. The minimum value CEP = 0.82 m was obtained at launch angle Θ_0 = 20° for T_{sk} = 900 N and Θ_g = −10°. For an unguided projectile launched at Θ_0 = 20°, the CEP was 216.62, so the reduction ratio (unguided projectile CEP/ guided CEP) is ≅ 264. This proves that the guidance law could significantly reduce the dispersion when compared to an uncontrolled projectile. The map for launch angle 20° (Figure 20a) is different from the others and the dispersion depends equally on both parameters. For elevation angles between 30° and 50°, the CEP reduction depends mainly on thruster magnitude and to a lesser extent on the parameter Θ_g. The results of the analysis indicate that the thruster magnitude should be at least 700 N (28 Ns). On the other hand, the thrust force cannot be too high because, as shown in Figure 12a,b, this can lead to high oscillations in the total angle of attack. The optimum value of threshold pitch angle Θ_g is between 0° and −15°.

3.3. INS Errors Influence on the Guidance Process

In the next step, the gyroscope and accelerometer noises were introduced to the developed model and a series of simulations was evaluated. The differences between "true" and measured orientation and position for launch angle 50° are presented in Figure 21.

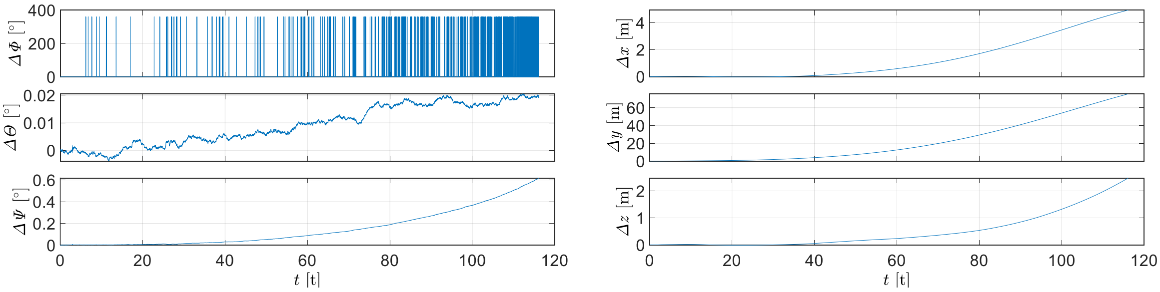

(**a**) (**b**)

Figure 21. INS errors (**a**) orientation (**b**) position (launch elevation angle 50°).

The orientation and position errors vary with time and are the biggest at the end of the flight. The largest angular difference was observed for the yaw angle. These results show that navigation errors cannot be ignored during the guidance process.

Next, the influence of INS errors on CEP was investigated. The lateral thruster magnitude was assumed to be T_{sk} = 700 N and Θ_g = 0°. The resulting hitting patterns for several launch tube elevations are presented in Figure 22.

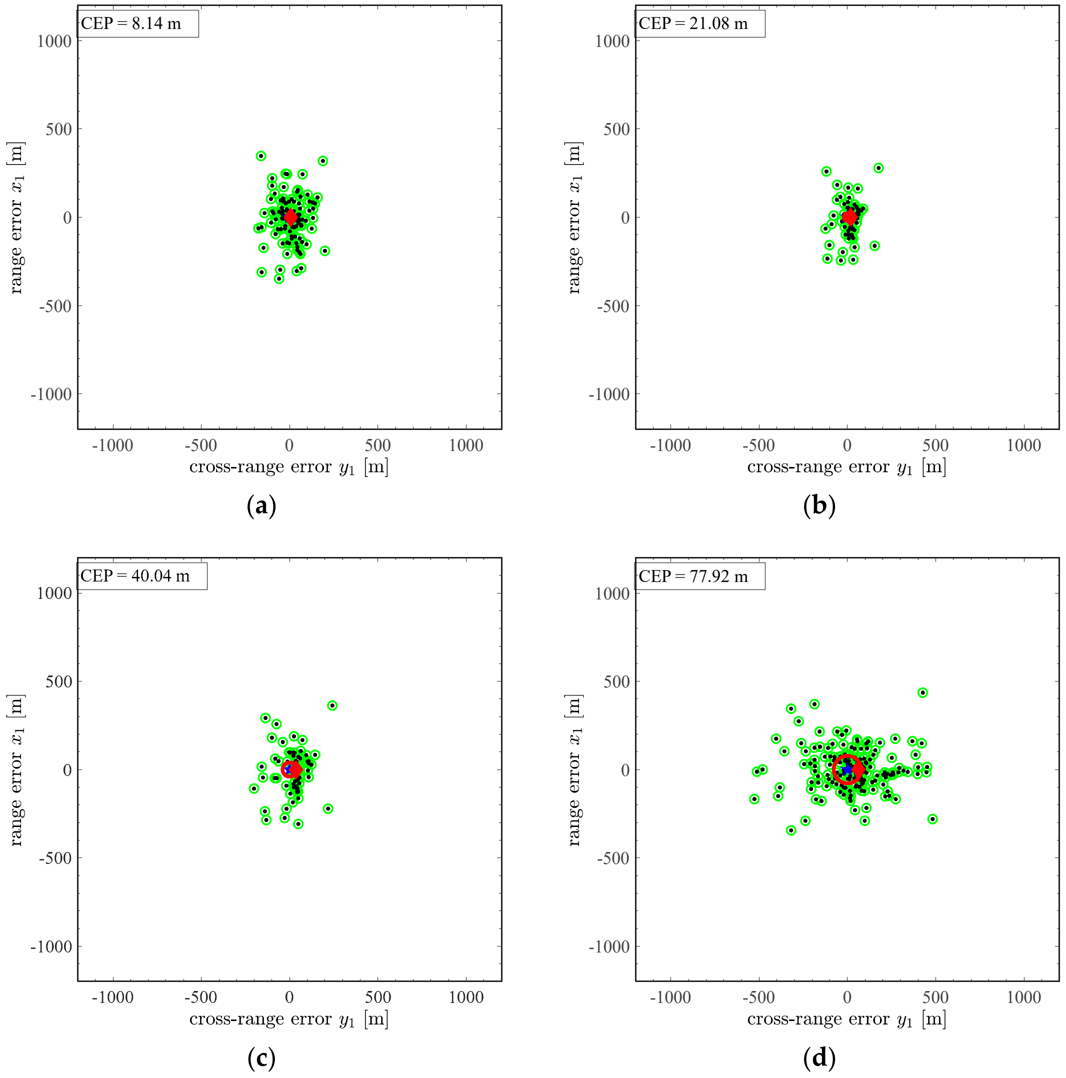

(**a**) (**b**)

(**c**) (**d**)

Figure 22. Hitting patterns for various nominal launch angles (**a**) Θ_0 = 20° (**b**) Θ_0 = 30° (**c**) Θ_0 = 40° (**d**) Θ_0 = 50° (controlled with INS noise).

The comparison between CEP for ballistic, controlled "ideal" and IMU noised simulation scenarios is presented in Table 2.

Table 2. Projectile CEP for various simulation scenarios.

Simulation Scenario	**Ballistic Flight**	**Controlled (without INS Noise)**	**Controlled (with INS Noise)**
Launch Angle [°]		**CEP [m]**	
20	216.62	3.16	8.14
30	239.58	7.22	21.08
40	309.94	10.02	40.04
50	358.74	5.15	77.92

The changes in CEP for the guided projectile without considering INS noise are quite small and the greatest value is no more than 10.02 m, which means that the formulated accuracy requirement is met at each elevation angle. The dispersion for a controlled flight with INS noise increases with the elevation angle because the flight time is longer for greater launch angles. This result is typical for IMU-only-based navigation systems, in which there is square growth of position errors in time.

The CEP for INS errors is still smaller than for unguided scenarios but also greater than for the idealized case. It was observed that navigation errors could affect the projectile dispersion significantly. When the INS noise was applied then the CEP at launch angle 20° is 8.14 m, but at 50° increases up to 77.92 m (9.57 times bigger than at 20°). At elevation 50°, for a guided projectile with the perfect INS, the CEP reduction ratio with respect to a unguided rocket is 69.6, but with the noise, the dispersion was reduced by only 4.6 times. It means that the accuracy of the INS system relevantly influences the resulting projectile dispersion and the navigation errors should be minimized in real applications. The location of the mean point of impact is shifted because the same kind of noise was used in each simulation sample.

3.4. Main Motor Thrust Curve Optimization

In a similar way, the main motor characteristics were considered, as these are variable and can be improved. The objective function was to extend the projectile range. This goal might be achieved by adding a propellant, which increases the projectile mass, or by modifying the shape of the thrust curve. It was assumed that the shape of the thrust curve remains the same in each simulation scenario. This means that the thrust magnitude and duration might be varied but the total impulse is held constant at 99624 N. The constraints have been imposed on the thrust curve. The minimum allowed operation time was set to 0.5 of the basic value and the maximum was set to 2.4. The launch angle was set to 50°. The projectile range as a function nondimensional burning time (actual/initial) was presented in Figure 23.

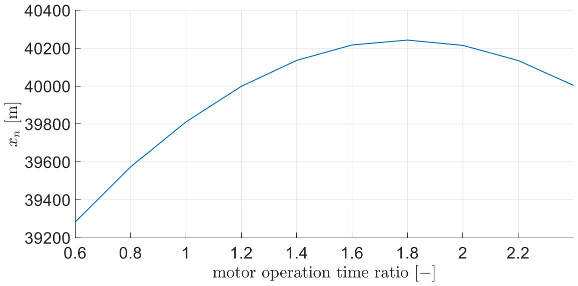

Figure 23. Projectile range for various main motor thrust magnitude and duration combinations.

The range initially increases with increasing the burning time of the propellant, but later the characteristic is flattened. It was found that the longest range is achieved when the motor operation time is 1.8 time longer than the initial value. The range was increased by 431.7 m with respect to initial configuration.

4. Conclusions

The purpose of this paper was to present a practical use of the Monte-Carlo simulation methodology for sensitivity analysis of the developed guidance algorithm. Impact point prediction guidance based on zero effort miss-distance extended with the trajectory shaping capability was implemented to increase the projectile accuracy and ensure a steeper angle of impact. In the described approach, a large number of disturbances was introduced to investigate the influence of various parameters on the guidance process. Quite short run times of the model (≅21 s per single simulation for elevation angle 50°) allow us to realize a large number of runs and investigate the influence of various parameters on guidance and control (G&C) quality. The thrust magnitude cannot be too high (>2000 N) because significant oscillations (up to 13.5°) in the total angle of attack might occur. The numerical results indicate that with the proposed guidance algorithm and perfect INS, CEP could be reduced by even ≅ 260 times when compared to an unguided projectile. The resulting CEP strongly depends on the lateral thruster magnitude, which should be at least 700 N (the total impulse of the single thruster 28 Ns) to nullify the miss distance. It means that the required total impulse from all 34 thrusters is 952 Ns. At launch elevation angle 20°, CEP depends in equal measure on the thruster magnitude and the threshold pitch angle Θ_g. On the other side, at higher launch angles, CEP varies mainly with thrust amplitude. The proposed augmented impact point prediction method requires quite a large number of lateral thrusters and high thrust magnitude. The algorithm robustness on INS errors was studied. It has been stated that the dispersion of the guided projectile strongly depends on the INS accuracy. When the noise from the real device was introduced, the dispersion is greater than in the idealized case and the CEP reduction ratio with respect to uncontrolled projectile at launch angle 20° is ≅26.6, and, at elevation 50°, only 4.6. The important practical aspect of the study is that control authority maps could be used to prepare flight experiments at the test range.

To highlight the superiority of the proposed guidance method, it is worth mentioning that most of the impact point prediction-based methods presented in the existing literature allow researchers to only to reduce the dispersion and do not possess trajectory shaping functionality. The distinguishing feature of the developed algorithm, comparing with others, lies in the fact that using lateral thrusters as actuators means that two control objectives could be realized simultaneously: miss distance minimization and angle of impact increasing. Assuming that the onboard navigation system could measure the projectile state precisely, even with the deactivation of first guidance phase (N_1 = 0), with the developed method high prediction convergency was obtained and a result of CEP < 10 m could be achieved. For example, Pavković [8] concluded that for a 262 mm thruster steered munition, the achieved CEP was 5.1 m and the CEP reduction ratio was 94.5, which is less than was obtained in this work. Guo [12] showed that for a 122 mm canard controlled projectile, CEP = 4.1 m, and the dispersion was reduced 113.7 times.

Further studies could concentrate on similar analyses for other system parameters (e.g., number of thrusters, operation time of the single thruster or nozzle location with respect to projectile center of mass) including also firing at a moving target. Also, more uncertainties (e.g., aerodynamics, environment) could be added to the model. Side jet interference effects should be included into the numerical simulation. A hardware-in-the loop test with a real INS system might be conducted to evaluate the system accuracy.

Author Contributions: Conceptualization, M.J.; formal analysis, R.G.; investigation, R.G. and M.J.; methodology, R.G. and M.J.; resources, R.G.; software, M.J.; supervision, R.G.; validation, M.J.; visualization, M.J.; writing—original draft preparation, M.J.; writing—review and editing, R.G. and M.J. All authors have read and agreed to the published version of the manuscript.

Funding: This research received no external funding.

Conflicts of Interest: The authors declare no conflict of interest.

Nomenclature

The following abbreviations and symbols are used in this manuscript:

Latin Symbols

C_X, C_Y, C_Z	axial, side and normal force aerodynamic coefficients, [-]
C_L, C_M, C_N	rolling, pitching and yawing moment coefficients, [-]
C_{LP}, C_{MQ}, C_{NR}	rolling, pitching and yawing damping moments coefficients, [-]
C_{X0}	drag force coefficient, [-]
d	projectile diameter, [m]
F	forces, [N]
g	gravity acceleration, [m/s^2]
i	number of the thruster, [-]
I	inertia matrix, [kgm^2]
$I_{xx0}, I_{yy0}, I_{zz0}$	projectile initial moments of inertia before main motor burnout, [kgm^2]

$I_{xxk}, I_{yyk}, I_{zzk}$	projectile initial moments of inertia after main motor burnout, [kgm^2]
m	projectile mass, [kg]
m_0	projectile initial mass, [kg]
m_k	projectile mass after main motor burnout, [kg]
M	moments, [Nm]
n	number of already fired thrusters, [-]
N	number of the lateral thrusters, [-]
N_1	number of thrusters used in the first guidance phase, [-]
P	roll rate, [°/s]
Q	pitch rate, [°/s]
r_{2t}	miss distance, [m]
r_{2tth}	miss distance threshold, [m]
R	yaw rate, [°/s]
S	projectile cross section area, [m^2]
t	time, [s]
t_g	guidance initialization time, [s]
t_{lt}	operation time of the single lateral thruster, [s]
t_{min}	minimum time between two consecutive firings, [s]
t_{prev}	time of the previous thruster firing, [s]
T_{sk}	lateral thruster thrust amplitude, [N]
T_m	main motor thrust, [N]
$U,\ V,\ W$	projectile velocities in body fixed frame, [m/s]
V_0	total flight velocity, [m/s]
$x_{ablt}, y_{ablt},\ z_{ablt}$	non-rotating frame
x_{cg0}	center of mass position before main motor burnout (from the projectile base), [m]
x_{cgk}	center of mass location after main motor burnout (from the projectile base), [m]
x_{lt}	lateral thrusters position (from projectile base), [m]
$x_n,\ y_n,\ z_n$	coordinates of the projectile center of mass in $O_n x_n y_n z_n$ reference frame, [m]
x_p, y_p	predicted impact point of the projectile in $O_n x_n y_n z_n$ reference frame, [m]
x_t, y_t	target location in $O_n x_n y_n z_n$ reference frame, [m]
x_1, y_1	range and cross-range errors, []
Greek Symbols	
α_t	total angle of attack, [°]
γ	desired flight direction in body fixed frame $O_b x_b y_b z_b$, [°]
γ_d	commanded flight direction in non-rolling body fixed frame $O_{ablt} x_{ablt} y_{ablt} z_{ablt}$, [°]
γ_p	miss distance phase in target plane, [°]
$\Delta x, \Delta y$	range and cross-range miss distance, [m]
ε	angular tolerance of lateral thruster firing, [°]
Θ	pitch angle, [°]
Θ_g	pitch angle threshold for first guidance phase, [°]
Θ_{g1}	pitch angle threshold for second guidance phase, [°]
Θ_T	main motor thrust misalignment pitch angle, [°]
μ	mean value
ρ	air density, [kg/m^3]
σ	standard deviation
Φ	roll angle, [°]
Φ_i	angular location of the *i*-th lateral thruster, [°]
Ψ	yaw angle, [°]
Ψ_T	main motor thrust misalignment yaw angle, [°]
τ	minimum allowed time between two consecutive firings, [s]
τ_d	igniter delay, [s]
τ_{sk}	lateral thruster delay, [s]
Abbreviations	
CEP	Circular Error Probable [m]
DoF	Degree of Freedom

GPU	Graphic Processing Unit
G&C	Guidance and Control
IMU	Inertial Measurement Unit
INS	Inertial Navigation System
IPP	Impact Point Prediction
MPI	Mean Point of Impact
TT	Trajectory Tracking
TS	Trajectory Shaping

References

1. Saghafi, F.; Khalilidelshad, M. A Monte Carlo Dispersion Analysis of a Rocket Flight Simulation Software. In Proceedings of the 17th European Simulation Multiconference, Nottingham, UK, 9–11 June 2003.
2. Al-Garni, A.Z.; Kassem, A.H.; Abdallah, A.M. Aerodynamic-Shape Optimization of Supersonic-Missiles Using Monte-Carlo. *Int. Rev. Aerosp. Eng.* **2016**, *4*, 7–15.
3. Mihailescu, C.; Radulescu, M.; Coman, F. The Analysis of Dispersion for Trajectories of Fire-extinguishing Rocket. Recent Advances in Fluid Mechanics and Heat & Mass Transfer. In Proceedings of the 9th IASME/WSEAS International Conference on Fluid Mechanics & Aerodynamics (FMA '11), Florence, Italy, 23–25 August 2011; pp. 135–140.
4. Ilg, M.; Rogers, J.; Costello, M. Projectile Monte-Carlo Trajectory Analysis Using a Graphics Processing Unit. In Proceedings of the AIAA Atmospheric Flight Mechanics Conference, Portland, Oregon, USA, 8–11 August 2011. [CrossRef]
5. Ilg, M. *Guidance, Navigation, and Control System Simulations via Graphics Processor Unit*; Army Research Laboratory: Aberdeen Proving Ground, MD, USA, 2011.
6. Ilg, M. *Multi-Core Computing Cluster for Safety Fan Analysis of Guided Projectiles*; Army Research Laboratory: Aberdeen Proving Ground, MD, USA, 2011. [CrossRef]
7. Pavković, B. Research of Projectile Trajectory Correction Methods in Function of Their Range and Precision Enhancement. Ph.D. Thesis, University of Belgrade, Belgrade, Serbia, 2012.
8. Pavković, B.; Pavić, M.; Ćuk, D. Frequency-Modulated Pulse-Jet Control of an Artillery Rocket. *J. Spacecr. Rockets* **2012**, *49*, 286–294. [CrossRef]
9. Pavković, B.; Pavić, M.; Ćuk, D. Enhancing the Precision of Artillery Rockets Using Pulsejet Control Systems with Active Damping. *Sci. Tech. Rev.* **2012**, *62*, 10–19.
10. Pavić, M.; Pavković, B.; Mandić, S.; Zivković, S.; Ćuk, D. Pulse-frequency modulated guidance laws for a mortar missile with a pulse jet control mechanism. *Aeronaut. J.* **2015**, *119*, 389–405. [CrossRef]
11. Drescher, T.; Kreuzer, W.; Nielson, J. Rocket Trajectory Correction using Strap-on GPS Guided Thrusters. In Proceedings of the IEEE 1998 Position Location and Navigation Symposium (Cat. No.98CH36153), Palm Springs, CA, USA, 20–23 April 1996. [CrossRef]
12. Guo, Q.-W.; Song, W.-D.; Gao, M.; Fang, D. Advanced Guidance Law Design for Trajectory-Corrected Rockets with Canards under Single Channel Control. *Eng. Lett.* **2016**, *24*, 469–477.
13. Sahu, J.; Fresconi, F. Flight Behaviors of a Complex Projectile using a Coupled CFD-based Simulation Technique: Closed-loop Control. In Proceedings of the 34th AIAA Applied Aerodynamics Conference, Washington, DC, USA, 13–17 June 2016. [CrossRef]
14. Zhang, Y.; Gao, M.; Yang, S.; Fang, D. Optimization of Trajectory Correction Scheme for Guided Mortar Projectiles. *Int. J. Aerosp. Eng.* **2015**, *2015*. [CrossRef]
15. Guo, Q.-W.; Song, W.-D.; Wang, Y.; Lu, Z.-C. Guidance Law Design for a Class of Dual-Spin Mortars. *Int. J. Aerosp. Eng.* **2015**, *2015*. [CrossRef]
16. Gamble, A.; Jenkins, P. Low Cost Guidance for the Multiple Launch Rocket System (MLRS) Artillery Rocket. *IEEE Aerosp. Electron. Syst. Mag.* **2001**, *16*, 33–39. [CrossRef]
17. Fresconi, F. Control mechanism strategies for spin-stabilized projectiles. *Proc. Inst. Mech. Eng. Part G J. Aerosp. Eng.* **2010**, *224*, 979–991. [CrossRef]
18. Lichota, P.; Jacewicz, M.; Szulczyk, J. Spinning gasodynamic projectile system identification experiment design. *Aircr. Eng. Aerosp. Technol.* **2020**, *92*, 452–459. [CrossRef]

19. Burchett, B. Prediction of Swerving Motion of a Dual-Spin Projectile With Lateral Pulsejets in Atmospheric Flight. *Math. Comput. Model.* **2002**, *35*, 821–834. [CrossRef]
20. Frost, G.; Costello, M. Stability and Control of a Projectile with an Internal Rotating Disk. In Proceedings of the AIAA Atmospheric Flight Mechanics Conference and Exhibit, Austin, TX, USA, 11–14 August 2003. [CrossRef]
21. Elsaadany, A.; Wen-jun, Y. Accurate Trajectory Prediction for Typical Artillery Projectile. In Proceedings of the 33rd Chinese Control Conference, Nanjing, China, 28–30 July 2014; pp. 6368–6374. [CrossRef]
22. IMI Systems. Available online: http://www.imisystems.com/wp-content/uploads/2017/01/ACCULAR-1.pdf (accessed on 23 March 2020).
23. State Kyiv Design Bereau "LUCH". Available online: http://www.luch.kiev.ua/en/catalogue-of-product (accessed on 21 March 2020).
24. Gao, M.J.; Zhang, Y.; Yang, S.; Fang, D.Y. Trajectory Correction Capability Modeling of the Guided Projectiles with Impulse Thrusters. *Eng. Lett.* **2016**, *24*, 11–18.
25. Corriveau, D.; Berner, C.; Fleck, V. Trajectory Correction Using Impulse Thrusters for Conventional Artillery Projectiles. In Proceedings of the 23rd International Symposium on Ballistics: Ballistics 2007, Tarragona, Spain, 16–20 April 2007; pp. 639–646.
26. Robinson, J.; Berefelt, F. *On Guidance and Control for Guided Artillery Projectiles, Part 1: General Considerations*; FOI Swedish Defence Research Agency: Stockholm, Sweden, 2011.
27. Gagnon, E.; Lauzon, M. Course Correction Fuze Concept Analysis for In-Service 155 mm Spin-Stabilized Gunnery Projectiles. In Proceedings of the AIAA Guidance, Navigation and Control Conference and Exhibit, Honolulu, HI, USA, 18–21 August 2008. [CrossRef]
28. Jitpraphai, T.; Costello, M. Dispersion Reduction of a Direct-Fire Rocket Using Lateral Pulse Jets. *J. Spacecr. Rockets* **2001**, *38*, 929–936. [CrossRef]
29. Gupta, S.; Saxena, S.; Singhal, A.; Ghosh, A. Trajectory Correction Flight Control System using Pulsejet on an Artillery Rocket. *Def. Sci. J.* **2008**, *58*, 15–33. [CrossRef]
30. Jitpraphai, T.; Burchett, B.; Costello, M. A Comparison of Different Guidance Schemes for a Direct Fire Rocket With a Pulse Jet Control Mechanism. In Proceedings of the AIAA Atmospheric Flight Mechanics Conference and Exhibit, Guidance, Navigation, and Control and Co-located Conferences, Montreal, QC, Canada, 6–9 August 2001. [CrossRef]
31. Burchett, B.; Costello, M. Model Predictive Lateral Pulse Jet Control of an Atmospheric Rocket. *J. Guid. Control Dyn.* **2002**, *25*, 860–867. [CrossRef]
32. Gross, M.; Costello, M. Impact point model predictive control of a spin-stabilized projectile with instability protection. In Proceedings of the AIAA Atmospheric Flight Mechanics (AFM) Conference, Boston, MA, USA, 19–22 August 2013. [CrossRef]
33. Rogers, J. Stochastic Model Predictive Control for Guided Projectiles Under Impact Area Constraints. *J. Dyn. Syst. Meas. Control* **2015**, *137*. [CrossRef]
34. Tian, Z.K.; Yang, S.C.; Feng, D.L.; Yao, Y.Z. Modeling and Simulation of impact point prediction algorithm. *Appl. Mech. Mater.* **2013**, *347*, 438–442. [CrossRef]
35. Fresconi, F.; Ilg, M. Model Predictive Control of Agile Projectiles. In Proceedings of the AIAA Atmospheric Flight Mechanics Conference, Minneapolis, MN, USA, 13–16 August 2012. [CrossRef]
36. Park, W.; Yun, J.; Ryoo, C.-K.; Kim, Y. Guidance Law for a Modern Munition. In Proceedings of the International Conference on Control, Automation and Systems 2010, Gyeonggi-do, Korea, 27–30 October 2010. [CrossRef]
37. Slegers, N. Model Predictive Control of a Low Speed Munition. In Proceedings of the AIAA Atmospheric Flight Mechanics Conference and Exhibit, Hilton Head, SC, USA, 20–23 August 2007. [CrossRef]
38. Slegers, N. Predictive Control of a Munition Using Low-Speed Linear Theory. *J. Guid. Control Dyn.* **2008**, *31*, 768–775. [CrossRef]
39. Fresconi, F.; Cooper, G.; Costello, M. Practical Assessment of Real-Time Impact Point Estimators for Smart Weapons. *J. Aerosp. Eng.* **2011**, *24*, 1–11. [CrossRef]
40. Fairfax, L.D.; Vasile, J.D.; Strohm, L.; Fresconi, F. Trajectory Shaping for Quasi-Equilibrium Glide in Guided Munitions. In Proceedings of the AIAA Scitech 2020 Forum, Orlando, FL, USA, 6–10 January 2020. [CrossRef]

41. Pamadi, K.; Ohlmeyer, E. Evaluation of Two Guidance Laws for Controlling the Impact Flight Path Angle of a Naval Gun Launched Spinning Projectile. In Proceedings of the AIAA Guidance, Navigation, and Control Conference and Exhibit, Keystone, CO, USA, 21–24 August 2006. [CrossRef]
42. Corriveau, D.; Wey, P.; Berner, C. Analytical Model Development and Impulse Thrusters Pairing Guidelines for Trajectory Corrections of Spin-Stabilized Projectiles. In Proceedings of the 48th AIAA Aerospace Sciences Meeting Including the New Horizons Forum and Aerospace Exposition, Orlando, FL, USA, 4–7 January 2010. [CrossRef]
43. Corriveau, D.; Wey, P.; Berner, C. Thrusters Pairing Guidelines for Trajectory Corrections of Projectiles. *J. Guid. Control Dyn.* **2011**, *34*, 1120–1128. [CrossRef]
44. National Aeronautics and Space Administration. *U.S. Standard Atmosphere, 1976*; National Aeronautics and Space Administration: Washington, DC, USA, 1976.
45. Burchett, B. Predictive Optimal Pulse–jet Control for Symmetric Projectiles. In Proceedings of the AIAA Atmospheric Flight Mechanics Conference, AIAA SciTech Forum, National Harbor, MD, USA, 13–17 January 2014. [CrossRef]
46. Lichota, P.; Szulczyk, J.; Tischler, M.B.; Berger, T. Frequency Responses Identification from Multi-Axis Maneuver with Simultaneous Multisine Inputs. *J. Guid. Control Dyn.* **2019**, *42*, 2550–2556. [CrossRef]
47. Baranowski, L. Equations of Motion of A Spin-Stabilized Projectile for Flight Stability Testing. *J. Theor. Appl. Mech.* **2013**, *51*, 235–246.
48. Burchett, B.T. Genetic Algorithm Optimization of Hydra Pulse Jet Controller. In Proceedings of the AIAA Atmospheric Flight Mechanics Conference and Exhibit, Honolulu, HI, USA, 18–21 August 2008. [CrossRef]
49. Gao, M.; Zhang, Y.; Yang, S. Firing Control Optimization of Impulse Thrusters for Trajectory Correction Projectiles. *Int. J. Aerosp. Eng.* **2015**, *2015*. [CrossRef]
50. Fresconi, F. Guidance and Control of a Projectile with Reduced Sensor and Actuator Requirements. *J. Guid. Control Dyn.* **2011**, *34*. [CrossRef]
51. Liu, F.; Su, Z.; Zhao, H.; Li, Q.; Li, C. Attitude Measurement for High-Spinning Projectile with a Hollow MEMS IMU Consisting of Multiple Accelerometers and Gyros. *Sensors* **2019**, *19*, 1799. [CrossRef] [PubMed]
52. Matsumoto, M.; Nishimura, T. Mersenne twister: A 623-dimensionally equidistributed uniform pseudo-random number generator. *ACM Trans. Model. Comput. Simul.* **1998**, *8*, 3–30. [CrossRef]
53. Driels, M. *Weaponeering: Conventional Weapon System Effectiveness*; American Institute of Aeronautics and Astronautics: Reston, VA, USA, 2013.